Evan Gawlik
SURF 2008 August Progress Report
Mentor: Dr. J. E. Marsden, Control and Dynamical Systems

SURF 2008 August Progress Report

Titan Mission Trajectory Design

1 Introduction

This report focuses on two topics: trajectories in the Sun-Earth-Moon system, and the design of a Multi-Moon Orbiter for the Saturnian moon system. Section 2.1 delivers a revised presentation of the results given in the previous progress report [1] on the application of DMOC to the design of a low-fuel trajectory from the Earth to the Moon. A brief discussion of the choice of a cost function for the "Shoot the Moon" trajectory optimization problem is also given. Section 2.2 offers insight into the role that invariant manifolds play in the "Shoot the Moon" trajectory by displaying results of Lagrangian coherent structure computations for the Sun-Earth-Moon-spacecraft four-body problem. In Sections 3.1 and 3.2, attention is shifted to the Titan mission trajectory design problem, where we discuss periodic orbits in the Saturn-Titan spacecraft system (Section 3.1) and make headway on the task of employing resonant gravity assists for the design of a Saturnian moon tour (Section 3.2).

2 DMOC, LCS, and the Sun-Earth-Moon System

2.1 Trajectory Optimization: Shoot the Moon

A number of factors discredit the results presented in the last progress report [1], most notably a mistake in the coded equations of motion used to generate trajectories and an improper conversion from normalized to dimensional units in the reported delta-V requirements of those trajectories. Here we deliver a revised presentation of the results of [1].

Recall the main goal of Progress Report #1 [1]: generate an optimal solution to the "Shoot the Moon" problem, the task of constructing a low-fuel trajectory from the Earth to the Moon. To recapitulate our approach, we aim to design an Earth-to-Moon trajectory (see Fig. 1) which traces the following route: (1) Depart Earth along a trajectory destined to nearly wind onto a Sun-Earth L_2 periodic orbit, (2) "bounce" off of the Sun-Earth L_2 equilibrium region along a path which hugs the unstable manifold of that Sun-Earth L_2 periodic orbit, and (3) enter the stable manifold tube of an Earth-Moon L_2 periodic orbit and achieve ballistic capture at the Moon. Trajectory optimization is to be accomplished through the use of the DMOC (Discrete Mechanics and Optimal Control) algorithm [2].

We shall impose the following boundary conditions on the spacecraft's trajectory: a fixed initial position and velocity which is destined to make a close approach of the Earth under the backward time flow, and a flexible final position and velocity which is required to satisfy the following family of constraints:

$$\frac{R_M + 200}{L_{SE}} \leq \sqrt{(x(t_f) - x_M(t_f))^2 + (y(t_f) - y_M(t_f))^2} \leq \frac{R_M + 2000}{L_{SE}} \tag{1}$$

$$\dot{x}(t_f) - \dot{x}_M(t_f) = \frac{-\sqrt{\mu_M}(y(t_f) - y_M(t_f))}{(x(t_f) - x_M(t_f))^2 + (y(t_f) - y_M(t_f))^2)^{3/2}} \tag{2}$$

$$\dot{y}(t_f) - \dot{y}_M(t_f) = \frac{\sqrt{\mu_M}(x(t_f) - x_M(t_f))}{(x(t_f) - x_M(t_f))^2 + (y(t_f) - y_M(t_f))^2)^{3/2}} \tag{3}$$

Here $(x, y, \dot{x}, \dot{y})$ and $(x_M, y_M, \dot{x_M}, \dot{y_M})$ denote coordinates of the spacecraft and Moon, respectively, in a normalized Sun-Earth rotating coordinate system, t_f denotes the final time at the endpoint of the spacecraft's

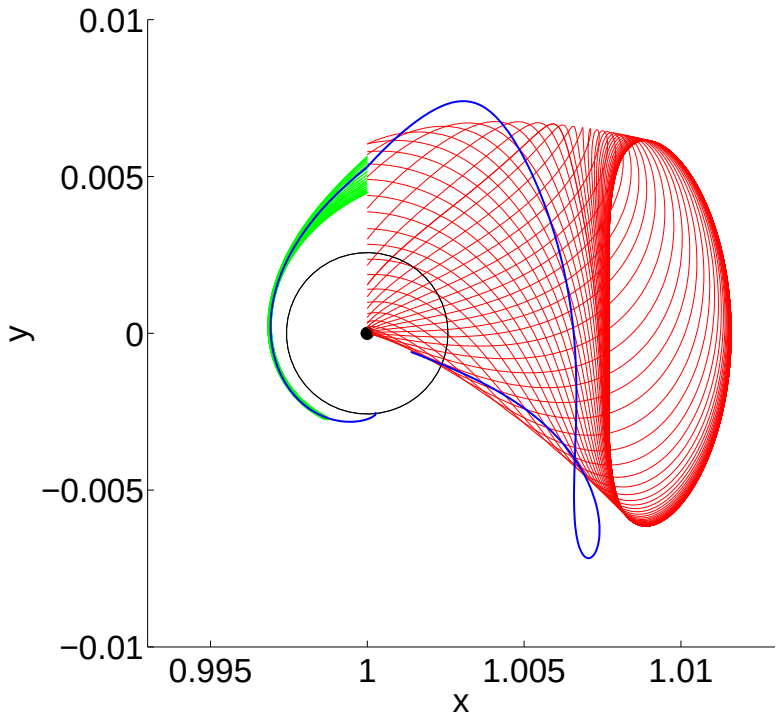

Figure 1: A patched Earth-to-Moon trajectory juxtaposed with the Sun-Earth (red) and Earth-Moon (green) invariant manifolds, in Sun-Earth rotating coordinates. The central black disc denotes the Earth, while the thin black circle traces the Moon's orbit. A ΔV of 163 m/s is required at the patch point.

trajectory, R_M and μ_M denote the radius and mass, respectively, of the Moon in normalized units, and L_{SE} is a conversion factor corresponding to the Sun-Earth distance in kilometers. Physically, constraints (1-3) correspond to the requirement that the spacecraft be in a 200- to 2000-km altitude circular orbit about the moon at time t_f.

One challenge associated with the application of DMOC to this trajectory design problem is the stiff nature of the four-body-problem equations of motion near the primary masses. Implicit in the DMOC algorithm is the use of a constant time-stepping numerical integrator. In general, small time steps are needed to ensure accuracy when simulating motion near the primary masses, but often large time steps can be used elsewhere without introducing noticable error. For trajectories which span both extremes in stiffness, a constant time-stepping integrator is impractical; sensitivities over short segments of the trajectory force the use of a small time step throughout the integration, leading to large computational costs.

For this reason, we split the trajectory in Fig. 1 into two pieces: a long segment that extends from Earth departure to a safe distance away from the Moon, and a short segment that spans the Moon arrival and capture phase of the trajectory. We use a large time step in the long, inital segment and a small time step in the short Moon arrival segment and require that the two pieces have matching (though not fixed) positions and velocities at their meeting point. To maximize flexibility, we leave the following parameters as

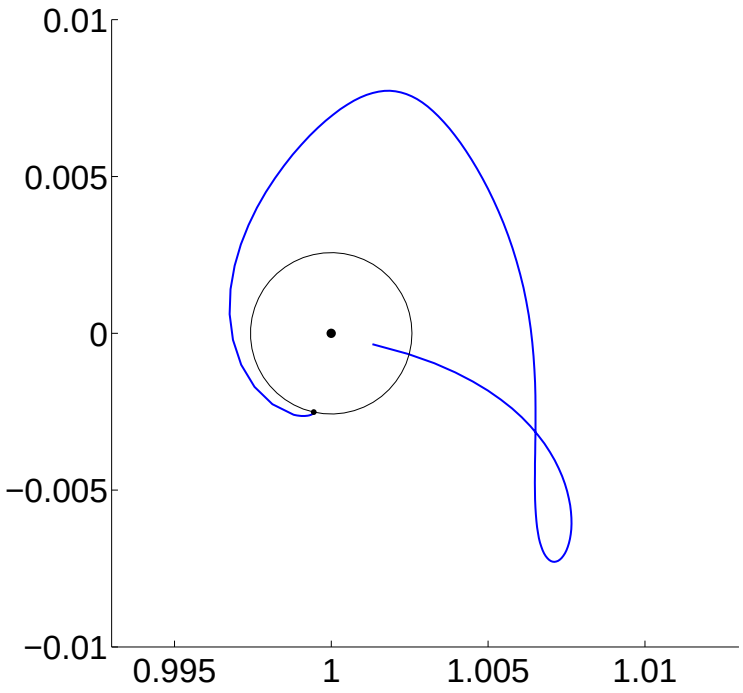

Figure 2: Locally optimal Earth-to-Moon trajectory (solid blue line). The central black disc denotes the Earth, while the thin black circle traces the Moon's orbit. A ΔV of 17 m/s is required for the optimal trajectory, a significant improvement over the patched trajectory's ΔV of 163 m/s.

optimizable control variables: the initial phase of the Moon, the time of flight, and the location and time at which the two trajectory pieces join.

The optimized trajectory generated through application of the DMOC algorithm is displayed in Fig. 2. The total ΔV requirement for this trajectory (excluding initial launch costs) is 17 m/s. This is roughly a tenfold improvement in the 163 m/s ΔV requirement for the patched trajectory of Fig. 1. These values differ from those reported in the previous progress report [1], where a combination of unit conversion errors and coding errors led to invalid results.

It is interesting to note that the use of different cost functions in the implementation of the DMOC algorithm can generate similar trajectories in position space with rather different *control trajectories* (and hence differing ΔV costs). The trajectory shown in Fig. 2 was generated using ΔV directly as the cost function to be minimized in the DMOC algorithm. Namely, this trajectory (locally) minimizes[1] the function

[1]In actuality, the sequential quadratic programming (SQP) routine used in this study generally does not converge when minimizing ΔV; if one continues to iterate the SQP routine the orbit remains nearly unchanged while the pulse of Fig. 3(a) becomes thinner and more sharply peaked.

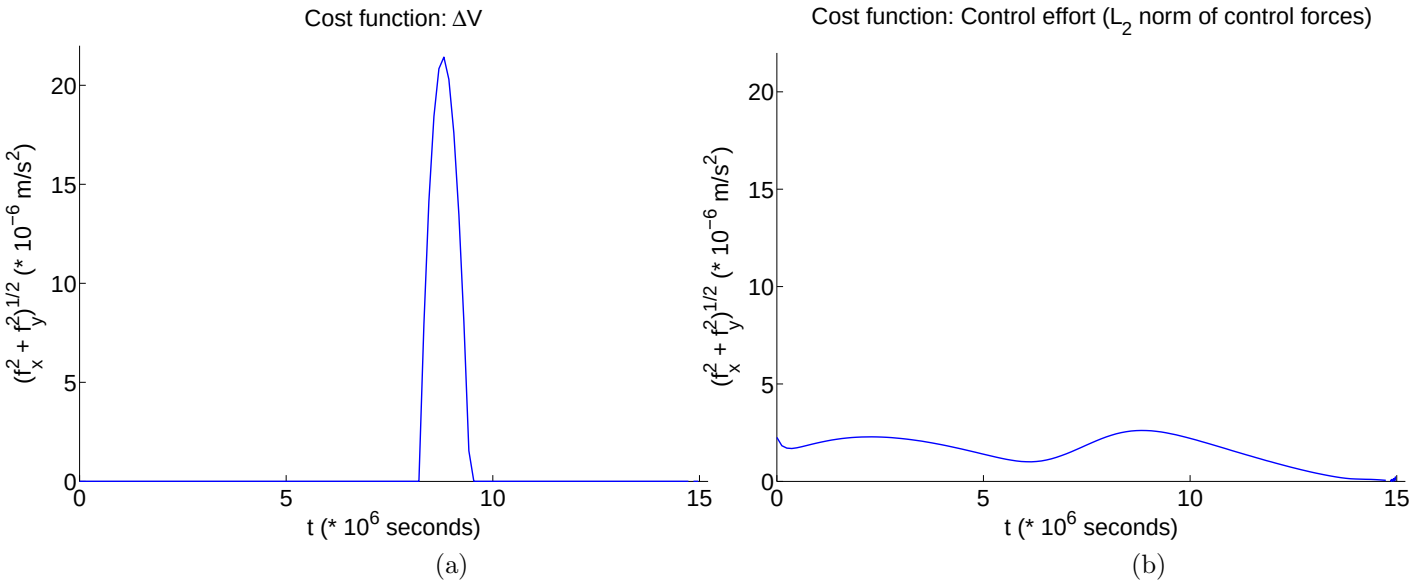

Figure 3: (a) Force vs. time for the Earth-to-Moon trajectory shown in Fig. 2, optimal with respect to the use of ΔV as a cost function. The forcing is heavily peaked over a short time interval and zero elsewhere, evidently a characteristic profile for minimal-ΔV orbits. (Note that the location of the peak is *not* at the patch point of the initial guess trajectory.) (b) Force vs. time for a minimal-control effort (L_2 norm of the control forces) trajectory from Earth to the Moon. The position space trajectory (not shown) is nearly identical to that of Fig. 2, but the control trajectory is strikingly different; namely, it is a smooth function of time. The total ΔV required for the minimal-ΔV and minimal-control effort orbits are 17 m/s and 23 m/s, respectively.

$$C(f) = \int_0^{t_f} ||f||\, dt \tag{4}$$

subject to the constraint that it satisfy Newton's laws and our imposed boundary conditions, where $f(t) = (f_x(t), f_y(t))$ denotes the control force applied at time t to steer the spacecraft. As shown in Fig. 3(a), the control trajectory $f(t)$ for this orbit takes the form of an impulse function, evidently a characteristic profile for minimal-ΔV orbits. For comparison, Fig. 3(b) shows the control trajectory when DMOC is applied using the "control effort" as a cost function:

$$\tilde{C}(f) = \int_0^{t_f} ||f||^2\, dt \tag{5}$$

In contrast to the minimal-ΔV control trajectory, the control trajectory for the minimal-control effort orbit is a smooth function of time.

2.2 Lagrangian Coherent Structures in the Four-Body Problem

Timing plays a key role in trajectory design. The initial launch time for the patched guess trajectory of Fig. 1 was carefully selected so that the phase of the moon would be such that the invariant manifolds

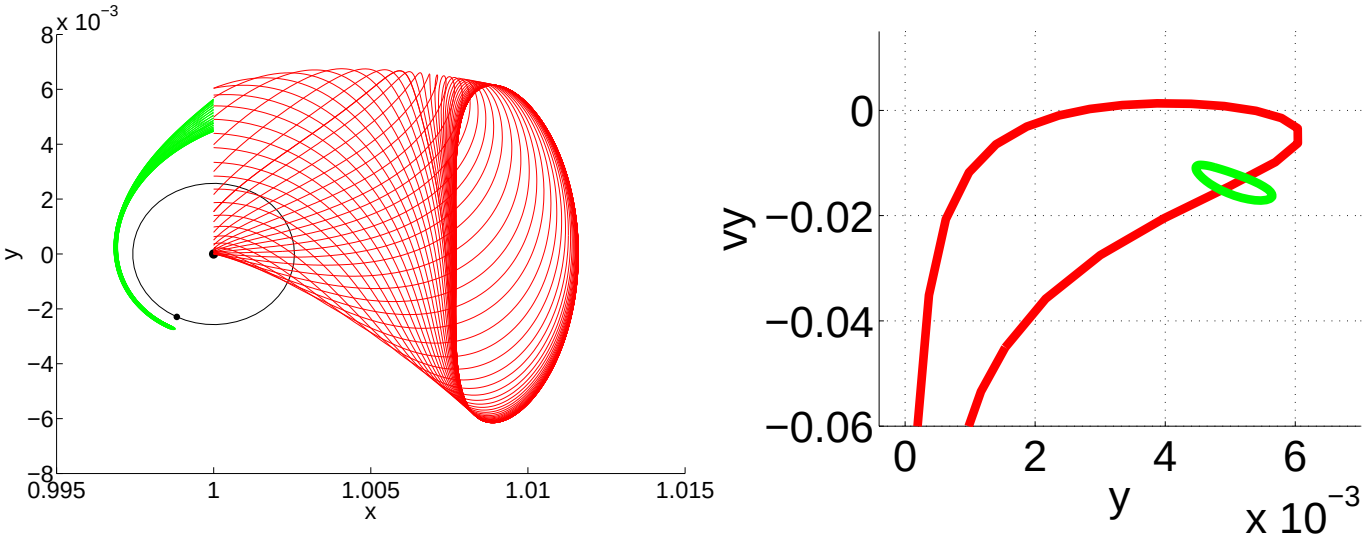

(a) (b)

Figure 4: (a) Unstable manifold (red) of an L_2 periodic orbit in the Sun-Earth-spacecraft three-body sytem, superposed with the stable manifold (green) of an L_2 periodic orbit in the Earth-Moon-spacecraft system. Coordinates are given with respect to a barycentric frame which rotates at a rate such that the Sun and Earth remain fixed on the x-axis. Units are scaled such that the Sun-Earth distance and the angular velocity of the rotating frame are both equal to unity. The central black disc denotes the Earth, while the thin black circle traces the Moon's orbit. (b) Intersection of the invariant manifold tubes depicted in (a) with the plane $x = 1 - \mu_E$, where $\mu_E = m_{Earth}/(m_{Sun} + m_{Earth})$.

of Fig. 4 intersect at the appropriate instant in time. The time dependence of these manifolds makes the four-body problem an ideal setting for an analysis of Lagrangian coherent structures. Fig. 5, together with an animated version in LCS-SEM.mov displays an LCS computed for the Sun-Earth-Moon system along the plane $\{(x, y, \dot{x}, \dot{y}) : x = 1 - \mu_E, E_{SE} = const.\}$, where μ_E is the mass parameter for the Sun-Earth system and E_{SE} denotes energy with respect to the Sun-Earth-spacecraft three-body system. As one should expect, this LCS (which corresponds to the stable manifold of an Earth-Moon L_2 periodic orbit shown in Fig. 4) glides across the plane as the initial phase of the moon varies. The most notable differences between the two figures are likely due to energy differences: In Fig. 4(b), the green lobe comprises trajectories who share a common three-body energy with respect to the Earth-Moon system. In contrast, the tracers used to generate the LCS in Fig. 5 were launched with a common three-body energy with respect to the Sun-Earth system.

3 Saturnian Moon Tours

3.1 Periodic Orbits in the Saturn-Titan-Enceladus System

In the design of NASA's mission to Titan, it is worthwhile to consider incorporating a periodic Saturnian orbit which makes flybys of both Titan and Enceladus, NASA's major targets for scientific study on the Titan mission. If such a trajectory has a period which matches an integer multiple of the Titan-Enceladus

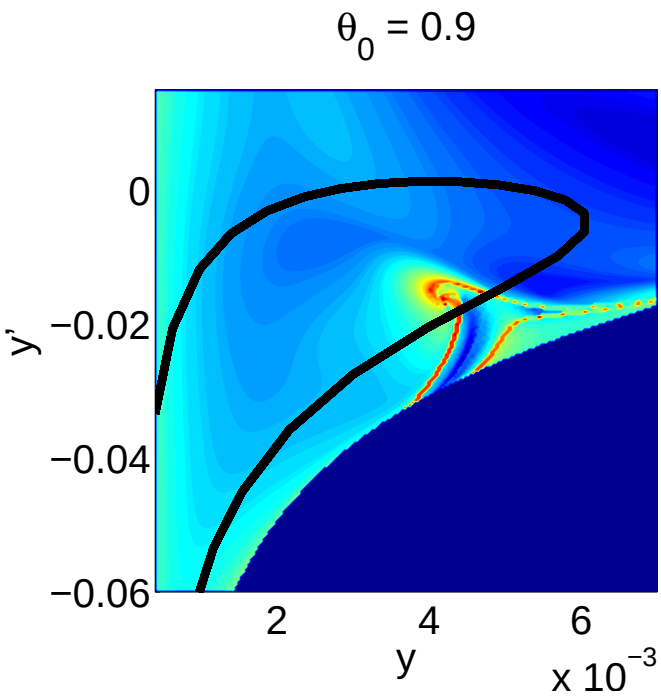

Figure 5: Snapshot of the Lagrangian coherent structures in the Sun-Earth-Moon-spacecraft four-body problem. The cross-section shown is the plane $x = 1 - \mu_E$ with a fixed value of the energy with respect to the Sun-Earth-spacecraft three-body system. For reference, the intersection of that plane with the unstable manifold of a Sun-Earth L_2 periodic orbit with a similar energy is displayed as a black curve. The LCS seen can be identified with the stable manifold of the Earth-Moon L_2 periodic orbit shown in Fig. 4. As the initial phase θ_0 of the Moon varies, the LCS glides across the plane, always encircling the lobe of trajectories destined to enter the sphere of influence of the Moon. See LCS-SEM.mov for an animation.

synodic period, it can be traversed as many times as needed to allow project managers to complete any desired number of moon flybys. In what follows, we adapt the methods of Ross [3] in order to reproduce the periodic Titan-Enceladus tours published by Russell and Strange [4] in an approximate model: namely, the Saturn-Titan-spacecraft circular restricted three-body problem.

Recall that the equations of motion for the circular restricted three-body problem (CR3BP) can be written

$$\ddot{x} - 2\dot{y} = \frac{\partial \Omega}{\partial x} \tag{6}$$

$$\ddot{y} + 2\dot{x} = \frac{\partial \Omega}{\partial y} \tag{7}$$

$$\Omega(x,y) = \frac{x^2+y^2}{2} + \frac{1-\mu}{\sqrt{(x+\mu)^2+y^2}} + \frac{\mu}{\sqrt{(x-1+\mu)^2+y^2}} + \frac{1}{2}\mu(1-\mu), \tag{8}$$

where $\mu = m_2/(m_1+m_2)$ is the mass ratio of two primary masses m_1 and m_2 moving in predefined circular

orbits about their center of mass, and x and y are the coordinates of a test particle m_3 with respect to a rotating coordinate frame in which m_1 and m_2 have fixed positions $(-\mu, 0)$ and $(1-\mu, 0)$, respectively [5]. Introducing the column vector $q = (x, y, u, v)'$ and identifying $\dot{x}$ with u and $\dot{y}$ with v, equations (6-7) can be recast as the first order system $\dot{q} = f(q)$, where

$$f(q) = \begin{pmatrix} u \\ v \\ 2u + \frac{\partial \Omega}{\partial x} \\ -2v + \frac{\partial \Omega}{\partial y} \end{pmatrix} \tag{9}$$

To produce a Titan-Enceladus cycler, we seek a periodic orbit in the Saturn-Titan-spacecraft three-body problem whose period is an integer multiple of the Titan-Enceladus synodic period, the relative period of Enceladus's orbit when viewed in the Saturn-Titan rotating frame:

$$T_{synodic} = \frac{2\pi}{\frac{T_T}{T_E} - 1} \tag{10}$$

Upon fixing such a period $T = mT_{synodic}$ $(m \in \mathbb{N})$, we can determine a periodic orbit with period T as follows: Assuming the orbit is symmetric about the x-axis, it suffices to find a trajectory which begins on the x-axis with zero velocity in the x-direction and terminates on the x-axis with zero velocity in the x-direction at time $t = T/2$. (This is a consequence of the symmetry $(x, y, \dot{x}, \dot{y}, t) \mapsto (x, -y, -\dot{x}, \dot{y}, -t)$ of the CR3BP equations of motion (6-7).) Suppose we start with a guess $q_0 = (x_0, 0, 0, v_0)'$ for the initial state along the periodic orbit. Then if $q(t)$ denotes the curve satisfying $\dot{q} = f(q)$ which passes through q_0 at $t = 0$, then we can write

$$q(T/2) = \phi^{T/2}(q_0), \tag{11}$$

where ϕ denotes the flow of the system $\dot{q} = f(q)$. That is, ϕ is the map satisfying

$$\frac{d\phi^t(q)}{dt} = f(\phi^t(q)) \tag{12}$$

$$\phi^0(q) = q \tag{13}$$

$$\tag{14}$$

for all state vectors q and all times t. In general, the vector $(x_f, y_f, u_f, v_f)' := \phi^{T/2}(q_0)$ will fail to satisfy the desired condition $y_f = u_f = 0$. We can target this desired state using differential correction to modify our initial guess q_0 by an amount $\delta q = (\delta x, \delta y, \delta u, \delta v)'$. To first order in δq, we can write

$$\phi^{T/2}(q_0 + \delta q) \approx \phi^{T/2}(q_0) + \Phi^{T/2}\delta q, \tag{15}$$

where $\Phi = \frac{\partial \phi}{\partial q}$ denotes the *state transition matrix* of the flow ϕ. Φ corresponds to the derivative of the flow with respect to initial position and satisfies the differential relation

$$\frac{d\Phi^t}{dt} = \frac{\partial f}{\partial q}\Phi^t \tag{16}$$

$$\Phi^0 = I, \tag{17}$$

$$\tag{18}$$

which can be derived by differentiating definition (12-13) with respect to q and noting symmetry of mixed derivatives.

Our goal is to adjust x_0 and v_0, while holding y_0 and u_0 fixed, so that the y- and u-components of $q(T/2)$ vanish. From relation (15), the y- and u-components of $\delta q_f := \Phi^{T/2}\delta q$ satisfy

$$\delta y_f = \Phi_{21}\delta x + \Phi_{24}\delta v \tag{19}$$
$$\delta u_f = \Phi_{31}\delta x + \Phi_{34}\delta v, \tag{20}$$
$$\tag{21}$$

where Φ_{ij} denotes the component of the matrix $\Phi^{T/2}$ in row i, column j. To target a final state with vanishing y- and u-components, we choose

$$\begin{pmatrix}\delta x\\ \delta v\end{pmatrix} = \begin{pmatrix}\Phi_{21} & \Phi_{24}\\ \Phi_{31} & \Phi_{34}\end{pmatrix}^{-1}\begin{pmatrix}-y_f\\ -u_f\end{pmatrix} \tag{22}$$

so that $\delta y_f = -y_f$ and $\delta u_f = -u_f$. If q_0 is sufficiently close to a true initial condition for a periodic orbit, then an iterative application of the map $q_0 \mapsto q_0 + \delta q$ as defined above typically converges to a solution within a few iterations.

The results of an application of the method just described to the computation of a periodic Titan-Enceladus cycler are shown in Fig. 6, along with an animated version in Titan-PO.mov. This trajectory corresponds to Titan-Enceladus cycler #314 from the database of Russell and Strange [4]. Over the course of its 49.5-day period, the orbit makes two flybys of Titan and one of Encaladus, provided the initial relative phase of Enceladus is chosen appropriately. Because its period is an integer multiple of the Titan-Enceladus synodic period (roughly 1.5 days), the orbit may be traversed as many times as needed to accomplish any desired number of moon flybys.

3.2 Resonant Gravity Assists

The low-fuel "Shoot the Moon" trajectory of Fig. 2 was made possible by a fortuitous intersection of the invariant manifolds of the Sun-Earth-spacecraft and Earth-Moon-spacecraft three-body systems. In a general celestial system, the distances between primary bodies and their relative masses may not permit such fortunate circumstances. In particular, it has been observed numerically that the invariant manifolds of the Saturn-Titan-spacecraft system do not pass near the invariant manifolds of the Lyapunov orbits associated with Saturn's other moons, a situtation that can be partly attributed to the small mass parameters of Saturn's non-Titanian moons.

To overcome this barrier, it is possible to utilize repeated gravitational assists to iteratively modify the osculating orbital elements of a spacecraft in orbit about Saturn and steer it toward sequential flybys at multiple moons. Such techniques have formerly been applied to the design of trajectories through the Jovian moon system which require very low amounts of fuel [6]. Dubbed a "Multi-Moon Orbiter," the trajectory begins in a Saturnian orbit with semimajor axis larger than Saturn's outermost major moon and performs resonant gravity assists with the major moons in sequence to gradually reduce the orbit's semimajor axis and visit multiple moons en route.

To facilitate the design problem, Ross and Scheeres [7] derive a map which approximates the change in orbital elements over the period of a particle in orbit in the exterior region of the circular restricted three-body problem with a small mass parameter μ. Given an orbit with Jacobi constant C_J, instantaneous Keplerian energy $K = -1/(2a)$ (where a denotes instantaneous semimajor axis), and argument of periapsis ω, the map approximates the orbit's change in Keplerian energy and argument of periapsis between successive arrivals at periapsis as

$$\begin{pmatrix}\omega_{n+1}\\ K_{n+1}\end{pmatrix} = \begin{pmatrix}\omega_n - 2\pi(-2K_{n+1})^{-3/2} \mod 2\pi\\ K_n + \mu f(\omega_n)\end{pmatrix}, \tag{23}$$

where f is the so-called *energy kick function* [7], a function depending parametrically on C_J and K which can be computed via numerical quadrature.

A plot of successive iterates of the Keplerian map for the Saturn-Titan system is given in Fig. 7. The image was generated by seeding a region of the (ω, K) cylinder with a 10×10 grid of points with Jacobi constant $C_J = 3.014$ and plotting their locations after 250 iterates of the map (23), where the parametric dependence of f on K was eliminated by fixing a reference Keplerian energy $\bar{K} = -0.3846$, an approximation advocated by Ross and Scheeres [7]. Included in Fig. 7(a) is a plot of the intersection of the stable manifold of an L_2 periodic orbit with the surface of section. The curve encloses a lobe of capture trajectories: sets of trajectories which, upon the next iterate of the Poincaré map, enter the Titan region of position space.

Ideally, we would like to find orbits which migrate from the upper portion of Fig. 7(a) to the lower portion and enter the green stable manifold tube. Such orbits, when plotted in position space, correspond to trajectories which start with a large semimajor axis, decrease in semimajor axis via the use of resonant gravity assists, and enter the stable manifold tube of a Saturn-Titan L_2 periodic orbit, a natural pathway leading to capture at Titan. The design of such a trajectory for the Jupiter-Callisto system, using a modified version of the Keplerian map (23) that incorporates control forces, has very recently been implemented by Ross, Jerg, and Junge [8]. The application of their method to the Saturn-Titan system will be the focus of my work in the forthcoming days.

References

[1] E. S. Gawlik. SURF 2008 July progress report: Titan mission design. *Caltech Summer Undergraduate Research Fellowship Progress Report*, pages 1–5, 2008.

[2] O. Junge, J. E. Marsden, and S. Ober-Blöbaum. Discrete mechanics and optimal control. In *Proceedings of the 16th IFAC Conference on Decision and Control*, pages 1–6, Prague, 2005.

[3] S. D. Ross. *Cylindrical manifolds and tube dynamics in the restricted three-body problem.* PhD thesis, California Institute of Technology, Pasadena, CA, 2004.

[4] R. P. Russell and N. J. Strange. Planetary moon cycler trajectories. *Journal of Guidance, Control, and Dynamics*, 2008.

[5] V. G. Szebehely. *Theory of Orbits: The Restricted Problem of Three Bodies.* Academic Press, New York, 1967.

[6] S. D. Ross, W. S. Koon, M. W. Lo, and J. E. Marsden. Design of a multi-moon orbiter. In *AAS/AIAA Space Flight Mechanics Meeting*, pages 1–15, Ponce, Puerto Rico, 2008.

[7] S. D. Ross and D. J. Scheeres. Multiple gravity assists, capture, and escape in the restricted three-body problem. *SIAM Journal on Applied Dynamical Systems*, 6:576–596, 2007.

[8] S. D. Ross, S. Jerg, and O. Junge. Optimal capture trajectories using multiple gravity assists. In *2nd Conference on Nonlinear Science and Complexity*, pages 1–6, Porto, Portugal, 2008.

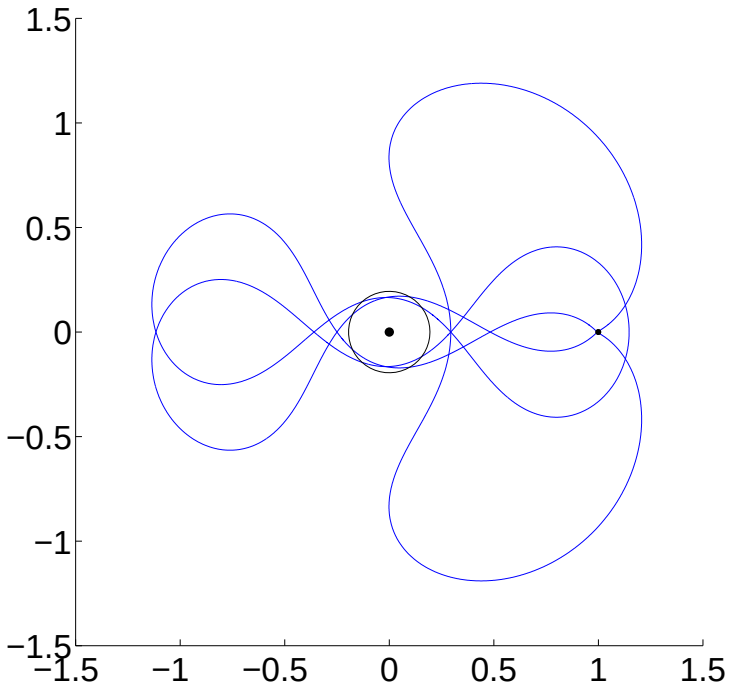

Figure 6: A periodic orbit in the Saturn-Titan-spacecraft three-body system, viewed in a rotating frame with Saturn and Titan fixed on the x-axis. The central black disc denotes the position of Saturn, the thin black circle traces Enceladus's orbit, and the outer black disc denotes the position of Titan. Over the course of its 49.5-day period, the orbit makes two flybys of Titan and one of Encaladus, provided the initial relative phase of Enceladus is chosen appropriately. Because its period is an integer multiple of the Titan-Enceladus synodic period (roughly 1.5 days), the orbit may be traversed as many times as needed to accomplish any desired number of moon flybys. The trajectory corresponds to Titan-Enceladus cycler #314 from the database of Russell and Strange [4]. See Titan-PO.mov for an animation.

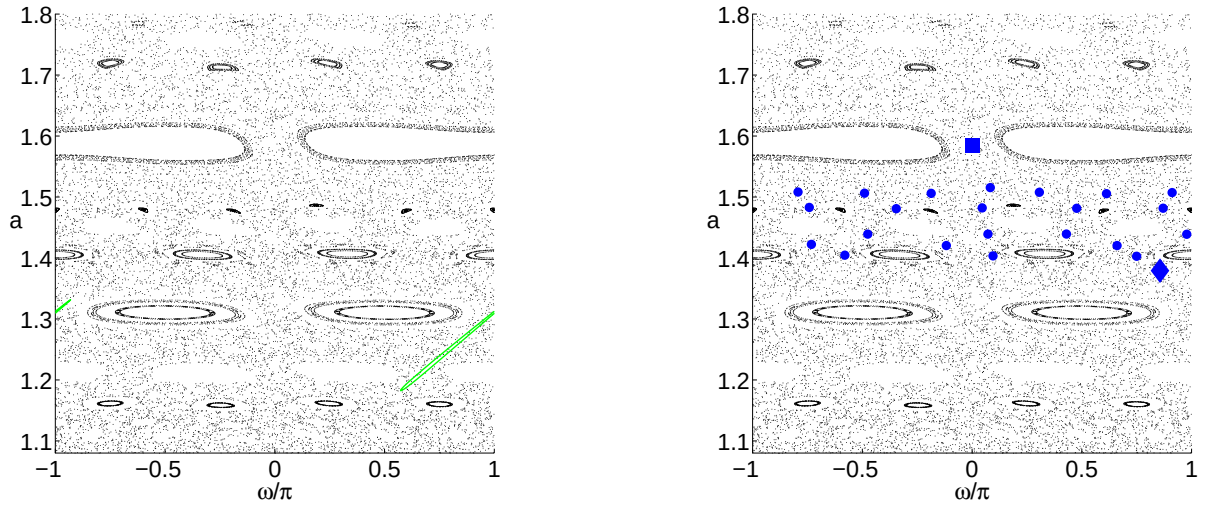

(a) (b)

Figure 7: (a) Poincare section taken at periapsis for orbits in the exterior region of the Saturn-Titan system, generated using the discrete Keplerian map (23). Axes are the instantaenous semimajor axis $a = -1/(2K)$ and argument of periapsis ω for the particle's orbit at the moment of periapsis. The green curve in the lower right-hand corner corresponds to the intersection of the stable manifold of an L_2 periodic orbit with the surface of section. The curve encloses a lobe of capture trajectories: sets of trajectories which, upon the next iterate of the Poincaré map, enter the Titan region of position space. (b) Example of a resonance-hopping trajectory in the Saturn-Titan system which quickly decreases its semimajor axis after several revolutions. The square and diamond denote the initial and final points, respectively, along the sequence of iterates marked in blue.